JOURNAL OF GEOPHYSICAL RESEARCH: SPACE PHYSICS, VOL. 118, 2340–2349, doi:10.1002/jgra.50197, 2013

Theoretical study: Influence of different energy sources on the cusp neutral density enhancement

Yue Deng,[1] Timothy J. Fuller-Rowell,[2] Aaron J. Ridley,[3] Delores Knipp,[2,4] and Ramon E. Lopez[1]

Received 22 January 2013; revised 21 February 2013; accepted 21 February 2013; published 3 May 2013.

[1] Simulations with the Global Ionosphere-Thermosphere Model (GITM) show that both Poynting flux and soft electron precipitation are important in producing neutral density enhancements near 400 km altitude in the cusp that have been observed by the Challenging Minisatellite Payload (CHAMP) satellite. Imposing a Poynting flux of 75 mW/m^2 in the cusp within the model increases the neutral density by 34%. The direct heating from 100 eV, 2 mW/m^2 soft electron precipitation produces only a 5% neutral density enhancement at 400 km. However, the associated enhanced ionization in the F-region from the electron precipitation leads to a neutral density enhancement of 24% through increased Joule heating. Thus, the net effect of the soft electron is close to 29%, and the combined influence of Poynting flux and soft particle precipitation causes a more than 50% increase in neutral density at 400 km, which is consistent with CHAMP observations in extreme cases. The effect of electron precipitation on the neutral density at 400 km decreases sharply with increasing characteristic energy such that 900 eV electrons have little effect on neutral density. Finally, the impact of 2 keV, 0.3 mW/m^2 proton precipitation on the neutral density is negligible due to a lowering of the altitude of Joule heating.

Citation: Deng, Y., T. J. Fuller-Rowell, A. J. Ridley, D. Knipp, and R. E. Lopez (2013), Theoretical study: Influence of different energy sources on the cusp neutral density enhancement, *J. Geophys. Res. Space Physics*, *118*, 2340–2349, doi:10.1002/jgra.50197.

1. Introduction

[2] *Lühr et al.* [2004], *Rentz and Lühr* [2008], *Rentz* [2009], and *Lühr and Marker* [2013] have presented the Challenging Minisatellite Payload (CHAMP) satellite observations of the thermospheric density in the cusp derived from high-resolution accelerometer measurements [*Reigber et al.*, 2002]. Typical enhancements in the cusp at 400 km altitude are 20% above background with a width of a few hundred kilometers; but in extreme cases, more than 50% have been observed. *Crowley et al.* [2010] also reported significant thermospheric density enhancements observed by CHAMP in the dayside cusp region during strong interplanetary magnetic field (IMF) B_y conditions, which can drive strong, localized ion drifts in the cusp region.

[3] *Lühr et al.* [2004] speculated that a local Joule heating fueled by ionospheric currents can be a driver because of the observed one-to-one correspondence between density peaks and the occurrence of fine-scale field-aligned current (FAC) filaments in this region. To explore the possibility that the Joule heating is responsible for the CHAMP-observed density enhancement in the cusp region, *Schlegel et al.* [2005] combined the currents measured on CHAMP with European Incoherent Scatter Scientific Association (EISCAT) measurements to estimate the Joule heating in the cusp. However, the results in *Schlegel et al.* [2005] show that the energy is small and the observed density enhancement has not been reproduced by the Thermosphere Ionosphere Mesosphere Electrodynamic General Circulation Model (TIMEGCM). *Demars and Schunk* [2007] successfully simulated a large density enhancement in the cusp using a thermospheric model for an idealized case. They increased the ion-neutral frictional heating in the cusp region by 110 times, which is difficult to reconcile with the observations. Based on results from the Assimilative Mapping of Ionospheric Electrodynamics (AMIE) [*Richmond*, 1992] procedure, *Crowley et al.* [2010] associated some of the significant thermosphere density enhancements observed by CHAMP in the dayside cusp region with strong interplanetary magnetic field B_y conditions. They showed a good agreement between the TIMEGCM-simulated neutral density and CHAMP observations at storm onset. However, the magnitude of the energy from AMIE outputs differed from the Poynting flux calculated from the Defense Meteorological Satellite Program (DMSP) magnetic and electric field data.

[4] Significant particle precipitation in the cusp region has been measured by both ground-based and satellite

[1]Department of Physics, University of Texas, Arlington, Texas, USA.
[2]CIRES, University of Colorado, Boulder, Colorado, USA.
[3]Department of AOSS, University of Michigan, Ann Arbor, Michigan, USA.
[4]High Altitude Observatory, NCAR, Boulder, Colorado, USA.

Corresponding author: Y. Deng, Department of Physics, University of Texas, Arlington, Texas, USA. (yuedeng@uta.edu)

2169-9380/13/10.1002/jgra.50197

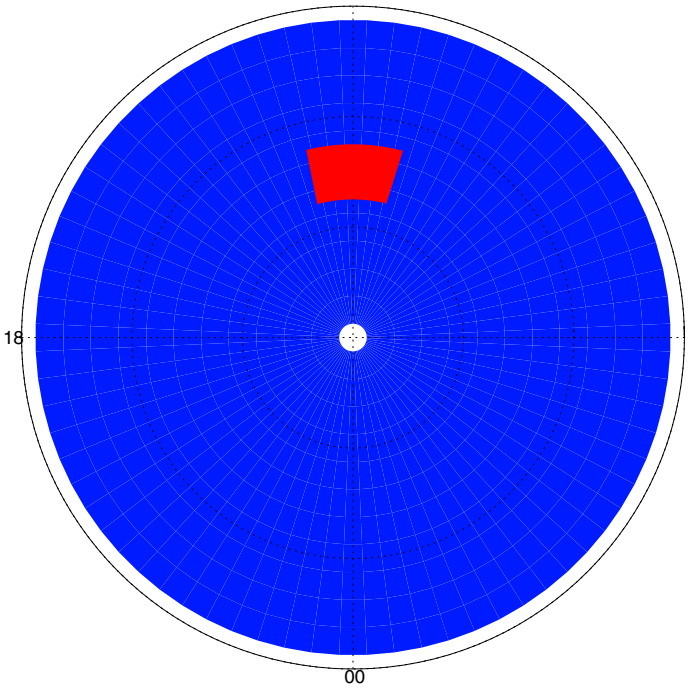

Figure 1. Schematic drawing of the simulated cusp region (72.5°N–77.5°N, 1100 LT–1300 LT), which is marked in the color of red. Uniformly distributed energy including Poynting flux and soft particle precipitation has been imposed in the cusp.

instruments [*Eather*, 1985; *Newell et al.*, 1989; *Smith and Lockwood*, 1996; *Escoubet et al.*, 2008], and some studies have been conducted to estimate the influence of the cusp precipitation on the ionosphere [*Millward et al.*, 1999; *Vontrat-Reberac et al.*, 2001; *Galand and Richmond*, 2001; *Prölss*, 2006; *Yordanova et al.*, 2007]. The CHAMP-EISCAT campaign [*Rentz*, 2009], which simultaneously observed the thermosphere with CHAMP and the ionosphere with the EISCAT incoherent scatter radar, revealed that the particle precipitation can also strongly influence the thermosphere by raising the effective altitude of the Joule heating. Conversely, measurement from the Streak mission at 250 km altitude presented a 1–2% density depletion related to the surrounding area [*Clemmons et al.*, 2008], which is quite different to the CHAMP's observations of a strong density enhancement at 400 km. *Clemmons et al.* [2008] suggested that this discrepancy can be explained by the relative difference of altitude effect between the soft particles in the cusp and harder particles in adjacent regions.

[5] Due to the limitations of the observations, the mechanism for the substantial neutral density enhancement in the cusp has not been confirmed previously, and no conclusive explanation for the neutral density enhancement has been agreed upon. To better understand the neutral density enhancement in the cusp, a comprehensive theoretical study of the heating mechanisms has been conducted using a global circulation model. Through a series of idealized simulations, we quantify the effect of different processes on the neutral mass density in the cusp at 400 km altitude. Specifically, the impacts of different heating processes including Joule heating, soft electron, and soft proton precipitation in extreme conditions are investigated.

2. Methodology

[6] The Global Ionosphere Thermosphere Model (GITM) is a three-dimensional spherical code that models the Earth's thermosphere and ionosphere system using a stretched grid in latitude and altitude [*Ridley et al.*, 2006]. It solves for the neutral and ion densities, velocities, and temperatures self-consistently. The most significant difference between GITM and other GCMs is that GITM does not assume a hydrostatic balance in the vertical direction. In addition, stretched grids in latitude and altitude are possible, and the number of grid points in each direction can be specified; so the resolution is flexible. GITM has been run at extremely high resolutions, such as 2.5° longitude by 0.375° latitude by one third scale height [*Yiğit and Ridley*, 2011]. One limitation of GITM is the small time step (2–3 s), due to its explicit solver and its ability to capture caustic wave [*Deng et al.*, 2008], while other hydrostatic implicit GCMs take much large time steps (2–5 min).

[7] The observations [*Newell and Meng*, 1992; *Zhou et al.*, 2000] indicate that the cusp source is averagely 1–2° in latitude and 2 h in local time. During some periods with large northward IMF Bz, the latitudinal width can be more than 4° [*Newell and Meng*, 1987; *Zhou et al.*, 2000]. Our simulation is to test the influence of the cusp heating to the neutral density during some extreme situations, which is close to the possible maximum. Therefore, the cusp region has been set to be 5° in latitude and 2 h in local time centered at 75°N, 1200 LT with a uniform distribution in our theoretical study as shown in Figure 1. To resolve such a feature, GITM model has been run at a resolution of 1° in latitude and 5° in longitude, which is higher than most

theoretical studies using GCMs [*Demars and Schunk*, 2007; *Zhang et al.*, 2012]. A uniform distribution of energy has been assumed, which is an oversimplification. Certainly, ignoring the spatial structure of the energy inputs inside the cusp can cause some quantitative difference from real events. Nevertheless, it is sufficient for our present study since it is an idealized exploration of the role of different energy inputs in the cusp region.

[8] A simple dipole magnetic field with the geomagnetic coordinates coincident with the geographic coordinates has been applied. The simulations are initialized with Mass Spectrometer Incoherent Scatter [*Hedin*, 1987] and International Reference Ionosphere [*Bilitza*, 2001] models with winds set to zero. The inputs into GITM include F10.7, Hemispheric auroral Power (HP), interplanetary magnetic field (IMF), and solar wind conditions. The F10.7 index is used as a proxy to specify the EUV spectrum that is subsequently used to calculate the solar ionization, dissociation, and heating of the atmosphere. The HP index is utilized to drive the *Fuller-Rowell and Evans* [1987] empirical model, which specifies the particle precipitation patterns for GITM. The IMF and solar wind plasma values are required as inputs to the *Weimer* [1996] empirical model, which specifies the electrodynamic potential patterns at high latitudes and drives the field-perpendicular ion flows.

[9] To initialize the simulation, GITM was first run for 24 h during the September equinox, reaching a quasi-steady state under relatively quiet conditions (IMF B_z =1.0 nT, HP= 15.0 GW, and F10.7= 100.0×10^{-22} W/m^2/Hz). Then, B_y was increased from 0 to 10 nT for 3 h. Since several hours are typical time period with large energy flux and particle flux during extreme cases, the simulations were compared 3 h after imposing the energy in the cusp, which is consistent with previous studies [*Demars and Schunk*, 2007; *Crowley et al.*, 2010]. The different heating processes (ions, electrons, and Poynting flux) were added in one-by-one and compared with the base case, to elucidate the relative importance of the various physical processes on the neutral density response. The empirical models were used to drive the high-latitude electrodynamics, from which the background Joule heating was calculated out. However, the strong feature within the cusp region were not well preserved in the empirical models, and the additional Poynting flux was imposed in the cusp at the top of the ionosphere and distributed in altitude using the Pederson conductivity to proportion it. Since the magnetic field lines are equipotential and are roughly perpendicular to the ground in the high-latitude region, the electric field is close to a constant in the vertical direction from the bottom of the model (100 km) to the top (600 km), and the Joule heating is proportional to the Pederson conductivity [*Thayer et al.*, 1995]. Also, given that the Poynting flux is a 2-D energy flux distribution at the top of the ionosphere/thermosphere, representing the altitude-integrated Joule heating, the Poynting flux is distributed in altitude by the vertical distribution of the Pederson conductivity. The altitude-resolved energy was then added on top of the background Joule heating, and the heating per unit volume is examined here. The particle precipitation cusp source was calculated from a given characteristic energy and total energy flux assuming a Maxwellian particle spectrum. The parameterization given by *Fang et al.* [2008] was utilized to determine the altitude profile of the soft electron ionization rate. The *Galand et al.* [1999] empirical model was used to specify the ionization rate associated with the proton precipitation.

3. Results and Discussion

3.1. Poynting Flux

[10] The unique characteristics of the cusp make it challenging to estimate the Joule heating directly from large-scale electric field and conductance measurements near this region. For example, the cusp is dominated by small-scale highly variable electric fields, for which the standard deviation is much larger than the average value. This has been illustrated by *Lühr et al.* [2004], which showed that averaging the FACs over 20 s reduced the amplitude of the current by about two orders of magnitude. Indeed, the Joule heating rate in *Schlegel et al.* [2005], calculated by combining measurements by CHAMP with EISCAT incoherent scatter radar measurements, was below 4 mW/m^2 and an order of magnitude smaller than that observed for storm conditions [*Vickrey et al.*, 1982]. Previous studies have shown that the electric field variability can significantly contribute to the estimation of the Joule heating [*Codrescu et al.*, 1995; *Matsuo et al.*, 2003; *Matsuo and Richmond*, 2008; *Rentz*, 2009]. Due to the importance of electric field variability, using the average electric field can result in a significant underestimation of the electromagnetic heating in the cusp.

[11] The Poynting flux $\left(S = \frac{<\mathbf{E}\times\Delta\mathbf{B}>}{\mu_0}\right)$ supplies one possible way to estimate the height-integrated Joule heating by application of Poynting's theorem [*Kelley et al.*, 1991; *Richmond*, 2010]. *Kelley et al.* [1991] explained that it could be applied to any high-latitude magnetic flux tube. *Weimer* [2005] also showed that in certain circumstances, the local downward component of Poynting flux above the ionosphere is dissipated entirely along that magnetic field line in the ionosphere below. *Richmond* [2010] proposed the equipotential Boundary Poynting flux theorem, which says that the area-integrated downward normal component of the Poynting flux, for a surface above the ionosphere that is bounded on the sides by an intersecting equipotential surface, equals the integrated electromagnetic energy dissipation in the volume bounded by those surfaces and by the base of the ionosphere.

[12] The downward Poynting flux is typically obtained from the vector cross product of the electric and perturbation magnetic fields measured in space [e.g., *Kelley et al.*, 1991; *Gary et al.*, 1995]. *Knipp et al.* [2011] showed an example of Poynting flux calculated from the measurements of the electric and magnetic fields along a DMSP F15 satellite trajectory on 25 August 2005. For that particular event, values of Poynting flux exceeded 100 mW/m^2 (erg/cm^{2}s) in and near the cusp during an interval of large IMF B_y. For our cusp simulation, a uniform Poynting flux of 75 mW/m^2 was imposed at the top of the thermosphere (Figure 1). The Poynting flux was roughly 20 times that of the altitudinally integrated Joule heating calculated with the empirical model (3–4 mW/m^2), but significantly less than the two orders of magnitude Joule heating enhancement introduced by *Demars and Schunk* [2007]. The imposed Poynting flux values are consistent with the Joule heating values derived

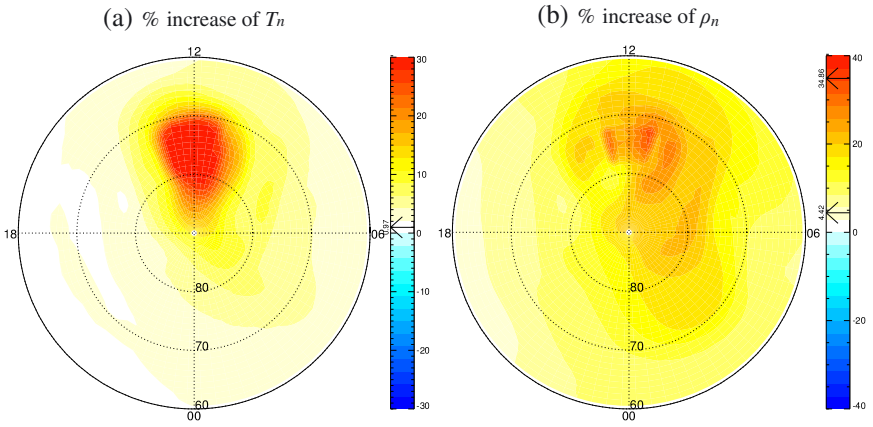

Figure 2. Difference in the thermosphere 3 h after adding in the Poynting flux (75 mW/m^2) in the cusp. (a) The percentage difference of neutral temperature at 400 km in the northern hemisphere between the cases with/without the additional Poynting flux. (b) The percentage difference of neutral density.

from MHD simulations of the large IMF B_y events described in *Li et al.* [2011].

[13] Figure 2a shows the percentage difference of neutral temperature at 400 km altitude between the cases with and without the additional Poynting flux in the cusp. Three hours after initializing the energy inputs, the neutral temperature in the cusp has increased by more than 30%. The elevated temperature region corresponds very well with the enhanced energy region, although it is somewhat more extended, especially towards the pole and to the west. Due to the increase in temperature and the subsequent thermal expansion of the thermosphere (as partially indicated by the vertical wind in Figure 3), the neutral density changes significantly. As shown in Figure 2b, the maximum percentage increase of neutral density is 34% at 400 km. The large enhancement indicates that Joule heating is definitely one of the major heating mechanisms in the cusp. Interestingly, the region with large density disturbance (> 20%) does not coincide exactly with the region of large temperature disturbance. These differences between density and temperature are due to the influence of both the horizonal and vertical winds on the neutral density distribution [*Fuller-Rowell et al.*, 1984; *Demars and Schunk*, 2007]. The density increase at dawn represents the nonlocalized effect of the cusp heating, due to background and perturbation neutral winds. When the energy is deposited in the cusp region, it causes the density to increase locally. This localized increase in density will (a) be redistributed by the background wind pattern and (b) alter the wind pattern, diffusing the strong gradients in the density. Because the IMF during this time is strong B_y

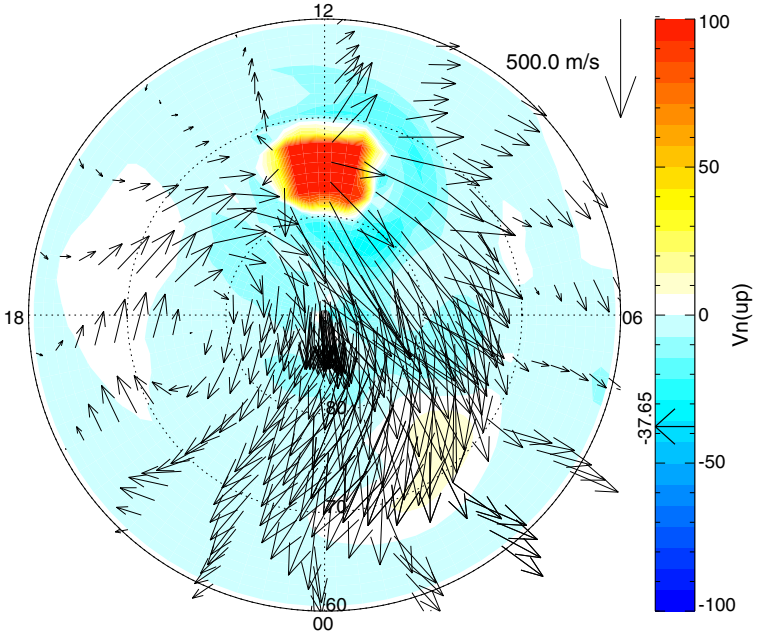

Figure 3. The distributions of the horizontal (vectors) and vertical (color contours) neutral wind after imposing the Poynting flux in the cusp.

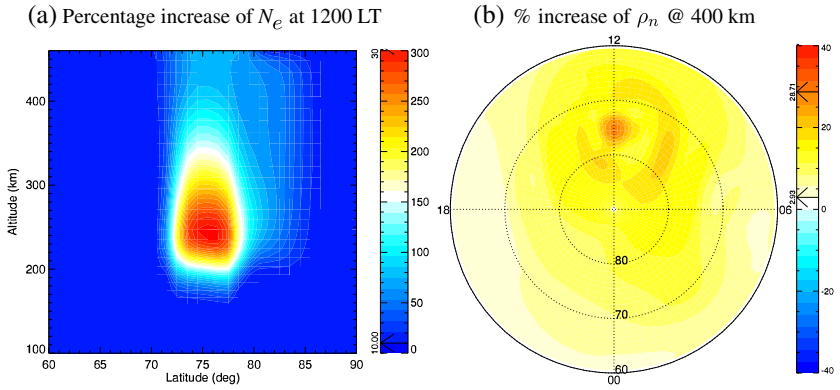

Figure 4. (a) The altitude-latitude distribution of the percentage increase of electron density at 1200 LT when the soft electron precipitation (100 eV, 2 mW/m^2) is imposed in the cusp. (b) The percentage change of the neutral density at 400 km altitudes caused by the soft electron precipitation.

positive, the winds in the cusp region are mostly in north-west direction as shown in Figure 3, which means that the density increase (or temperature increase) will be advected out of the cusp towards the north-west, which is exactly what is seen in Figure 2b. The percentage change of neutral density at 400 km (34%) is smaller than the percentage increase ($\sim$ 50%) from the CHAMP satellite measurements in the extreme cases [*Schlegel et al.*, 2005], and therefore, an additional heating mechanism is most likely required to explain the observations.

[14] Figure 3 presents the distribution of neutral wind when adding in the Poynting flux. There is an upwelling with an approximately 100 m/s upward neutral wind in the cusp and a downwelling with a 37 m/s downward neutral wind on the morning (west), north and south sides of the cusp. The asymmetry between the morning and afternoon sides of the cusp are most likely due to the prevailing neutral winds. Strong vertical wind, even as large as 100 m/s have been observed previously by Dynamics Explorer 2 (DE 2) satellite [*Innis and Conde*, 2002] and Fabry-Perot interferometers (FPI) measurements [*Smith and Hernandez*, 1995; *Aruliah et al.*, 2005] in the auroral zone. In addition, a neutral fountain structure with a downwelling next to an upwelling after an intense energy enhancement in a limited region has also been simulated previously [*Fuller-Rowell et al.*, 1984; *Demars and Schunk*, 2007] and explained as the consequence of advection change. The vectors in Figure 3 represent the horizontal neutral winds, which show a dominant dusk cell under the strong positive B_y condition. Additionally, the neutral wind is blowing out of the cusp region, which produces the eastward wind on the afternoon side and sunward wind on the equatorward side of the cusp. This is caused by the heating added in the cusp, which changes the pressure gradient and the neutral wind direction. Actually, the sunward wind has also been observed by the balloon-borne Fabry-Perot interferometer (FPI) at the equatorward of the cusp on the dayside [*Wu et al.*, 2012].

3.2. Soft Particle Precipitation

3.2.1. Soft Electron (100 eV)

[15] A significant amount of soft electrons with energies of 100 eV precipitate in the cusp region [*Burch*, 1968; *Frey*, 2007]. The flux of these soft particles is one to two orders of magnitude larger in the cusp than in the adjacent region [*Newell et al.*, 2009]. Through collisions, the soft electrons directly deposit heating at F-region altitudes [*Fontheim et al.*, 1987]. In addition, the soft electrons greatly increase the ionization and therefore conductivity above 150 km [*Millward et al.*, 1999; *Zhang et al.*, 2012], which changes the altitudinal distribution of the Joule heating and raises the height of the effective Joule heating [*Carlson et al.*, 2012]. The energy deposited in the F-region changes the neutral density at 400 km more efficiently than the energy deposited in the E-region [*Schunk and Nagy*, 2000]. Therefore, the impact on the neutral density at 400 km can be stronger in the cusp region than the adjacent area even though the total precipitation energy flux may be lower. In brief, the soft particle precipitation not only directly deposits heat into the upper thermosphere/ionosphere but also it changes the altitudinal distribution of the Joule heating.

[16] In some climatological particle precipitation models [*Fuller-Rowell and Evans*, 1987; *Roble et al.*, 1987], the low-energy cutoff is approximately 300–500 eV, and the soft particle precipitation is not included. The Kp-dependent auroral model, *Hardy et al.* [1987], does cover the energy range from 50 eV to 100 keV, but the cusp in this model is likely to be smeared out since it is basically a mesoscale feature. In the controlled case for this simulation, which is forced by the *Fuller-Rowell and Evans* [1987] empirical model, the soft particle precipitation was not been included. Therefore, an additional uniform distribution of soft electron precipitation has been imposed in the cusp region. According to the results in previous studies [*Newell et al.*, 1989; *Smith and Lockwood*, 1996; *Frey*, 2007; *Newell et al.*, 2009], the reasonable characteristic energy and energy flux during some extreme situations can be 100 eV and 2 mW/m^2, respectively. For simplicity, a uniform time and space distribution and the Maxwellian spectrum have been assumed in the simulations.

[17] Figure 4a illustrates the altitude-latitude distribution of the percentage increase of electron density at 1200 LT after adding in the soft electron precipitation. While the electron density below 150 km altitude barely changes, the electron density elevates at F-region altitudes, and the peak value is three times larger than the background. This altitudinal dependence is consistent with the fact that soft electrons

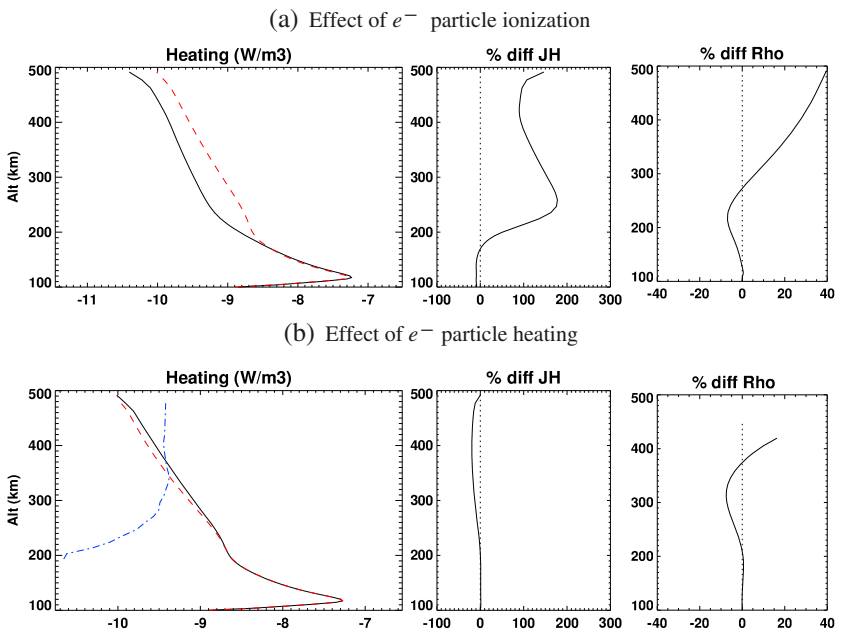

Figure 5. Comparison the two effects of soft electron precipitation (ionization and heating) on the neutral density. (a) The altitudinal profiles of the Joule heating (left) at 1200 LT, 75° latitude before (black) and after (red) including the ionization effect of soft electron precipitation. The percentage differences of the Joule heating and the neutral density have been shown in the middle and on the right. Figure 5b is the same as Figure 5a, except for the heating effect. The altitudinal profile of the particle heating is plotted out as blue line. The figures on the left panel are plotted on a logarithmic scale.

are absorbed almost entirely at F-region altitudes. The electron density enhancement is not limited to the defined cusp region (72.5°–77.5°); it actually spreads to higher latitudes due to the poleward plasma convection (∼ 1000 m/s) in the polar cap. Since the lifetime of ions in the F-region is relatively long [*Schunk and Nagy*, 2009], the electron density enhancement can be sustained for a considerable time even though the electrons have been transported away from the source region.

[18] The corresponding variation of the neutral density is shown in Figure 4b. At 400 km altitude, a neutral density enhancement with a peak of 29% occurred in the cusp region, which is comparable with the change of neutral density (34%) caused by the Poynting flux deposition, as shown in Figure 3. This implies that the soft electron precipitation is as important as the Poynting flux in contributing to the neutral density variation at 400 km. The altitude variation of the Joule heating is different when adding in the soft electrons since they cannot directly penetrate to the altitudes lower than 150 km. The electron density and Pedersen conductivity in the F-region are enhanced, as shown in Figure 4a, and more Joule heating is deposited in the F-region. If we assume that the height-integrated Joule heating is always equal to the Poynting flux at the top of ionosphere, which has been set as a constant in this study, then less Joule heating is deposited in the E-region. As a consequence, the influence of the soft particle precipitation on the neutral density at lower altitudes is negative in this simulation. While this study independently changes the electric field, Poynting flux, and particle precipitation, these processes are intimately linked in the magnetosphere-ionosphere-thermosphere coupled system [*Fedder and Lyon*, 1987; *Ridley et al.*, 2004]. It means that if the particle precipitation is increased, then there is a good chance that the magnetosphere will respond by reducing

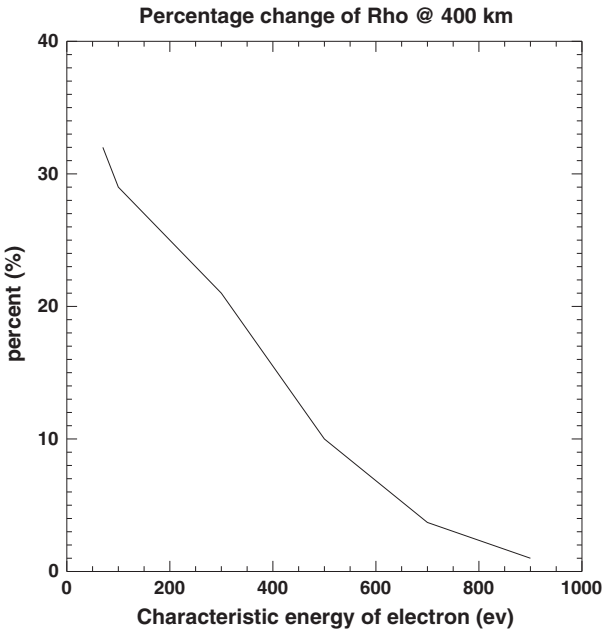

Figure 6. Maximum percentage change of neutral density at 400 km altitude caused by the soft electron precipitation with different characteristic energies.

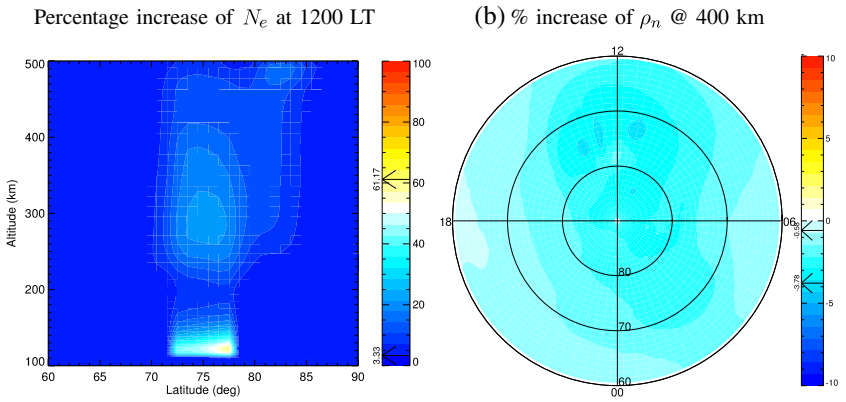

Figure 7. The same as Figure 4 except for the soft proton precipitation (2 keV, 0.3 mW/m^2).

the current, thereby reducing the electric field. This may cause a reduced effect from what is described here. The characteristic energy of the precipitating particles has a large role in this, since the energy specifies the altitude of the peak ionization and therefore the amount of conductivity enhancement. Lower particle energies, as shown here, cause ionization at higher altitudes, which will not cause as much enhancement in the height-integrated Pedersen conductivity; therefore, the feedback between the magnetosphere and ionosphere may be reduced, although this is not shown.

[19] Electron precipitation influences the upper atmosphere through two processes: directly depositing heat and increasing ionization. So far, many studies have been conducted examining the effect of direct heating on the thermosphere and ionization on the ionosphere individually [*Rees et al.*, 1983; *Fontheim et al.*, 1987; *Millward et al.*, 1999; *Vontrat-Reberac et al.*, 2001; *Prölss*, 2006]. However, much less attention has been paid to the influence of the ionization on the thermosphere in mediating the altitudinal distribution of the Joule heating when the particle precipitation and the Joule heating are coincident. Hence, the relative significance of the two processes, direct heating and ionization, to the neutral density enhancement at 400 km is still not clear. In order to investigate the contribution of each process, their effects have been separated through artificially turning them on one-by-one in the simulations. Figure 5a shows the altitudinal profiles of the Joule heating (left) at 1200 LT, 75° latitude before (black) and after (red) the particle ionization has been added. The percentage differences of the Joule heating and the neutral density are shown in the middle and on the right. Due to the change of ionization, the Joule heating increases above 170 km and decreases below that. The percentage difference of neutral density changes from negative to positive at 280 km, with a decrease of 7% at 220 km and an increase of 24% at 400 km, which is the bulk of the total contribution from soft electrons (29%).

[20] Figure 5b is the same as Figure 5a, except that it shows the effects of the direct soft particle heating (blue line) on the Joule heating and mass density. Since *Rees et al.* [1983] underestimates the neutral heating efficiency of the 100 eV electrons above 250 km [*Richards*, 2013], an adjustment of a factor of two has been applied in the heating calculation. The heating rate calculations in *Richards* [2013] differ from previous heating rate calculations in the treatment of backscattered electrons to produce better agreement with observed flux spectra. The neutral gas heating rates are therefore higher than when the backscattered flux escapes from the ionosphere. The direct particle heating becomes comparable with the Joule heating above 350 km. When including the direct particle heating, the Joule heating is reduced slightly above 250 km due to nonlinear ionosphere-thermosphere coupling. The particle heating increases the neutral temperature and therefore the ion recombination rate, which reduces the electron density and Pedersen conductivity. Consequently, the Joule heating also decreases in the F-region, which is presented in the percentage change of the Joule heating in the middle panel of Figure 5b. The combination of the direct particle heating enhancement and the Joule heating reduction causes the neutral density variation shown in the right panel of Figure 5b. The percentage difference of neutral density due to direct heating from the soft particle precipitation is close to 5% at 400 km altitude, which is much smaller than the density change caused by the ionization process (24%). Therefore, the ionization effect dominates the influence of the soft electron precipitation on the neutral density.

[21] The characteristic energy and total energy flux of the precipitating particles have been utilized to describe the Maxwellian particle energy spectrum and to calculate the particle ionization and heating rates. The electron precipitation with the same energy flux but different characteristic energies produces different altitudinal profiles of ionization and energy deposition rates [*Rees et al.*, 1983; *Fang et al.*, 2008; *Clemmons et al.*, 2008]. As a consequence, the effect on the neutral density also strongly depends on the characteristic energy of the particles. Figure 6 shows how the maximum change of neutral density at 400 km varies with the characteristic energy of the electrons. When the energy increases from 70 to 900 eV without changing the total energy flux (2 mW/m^2), the peak value of the neutral density variation decreases from 32% to 1%. The influence of 900 eV particles on the neutral density at 400 km is almost negligible. When the particles are more energetic, they penetrate deeper into the atmosphere [*Roble and Ridley*, 1987; *Millward et al.*, 1999; *Fang et al.*, 2008] and increase the Joule heating at lower altitudes. If the Joule heating energy deposition were the same, then the neutral gas heating rate would be lower, since the heating rate is the energy deposition rate divided by the mass density, which is larger at lower altitudes. In essence, the same amount of energy has to

heat up more particles, so the temperature change is smaller than if the same energy were deposited at higher altitudes. Therefore, the softer particles produce larger neutral density enhancement at higher altitudes which is a more efficient heating location.

3.2.2. Soft Proton (2 keV)

[22] In addition to the soft electron precipitation, there is a significant soft proton precipitation in the cusp [*Potemra et al.*, 1977; *Newell et al.*, 1989; *Smith and Lockwood*, 1996; *Millward et al.*, 1999; *Vontrat-Reberac et al.*, 2001]. The characteristic energy and the energy flux of the protons are close to 2 keV and 0.3 mW/m^2 in a geomagnetically active condition [*Newell et al.*, 1989; *Millward et al.*, 1999; *Vontrat-Reberac et al.*, 2001; *Frey*, 2007]. The *Galand et al.* [1999] empirical model has been used to specify the ionization rate associated with the proton precipitation. As shown in Figure 7a, the soft proton precipitation increases the electron density much more significantly in the E-region than in the F-region. It is consistent with previous studies [*Millward et al.*, 1999; *Vontrat-Reberac et al.*, 2001], which also reported that the influence of proton precipitation on the ionosphere is dominant below 200 km altitude. A maximum electron density change of 61% occurs at 120 km altitude, which is similar to the simulation results in *Galand et al.* [1999]. The variation of the electron density influences the thermosphere through changing the altitudinal distribution of the conductivity and the Joule heating [*Galand et al.*, 2001; *Galand and Richmond*, 2001]. As shown in Figure 7b, the net effect is for a 4% decrease in mass density at 400 km. The influence is therefore small compared with that produced by the Poynting flux or soft electron precipitation. Hence, soft proton precipitation is probably not a significant contributor to the energy budget or the density response at 400 km.

[23] Table 1 summarizes the influence of different heating mechanisms, including Poynting flux, soft electron precipitation, and soft ion precipitation, on the neutral density variation at 400 km. As shown in Figure 8, the combination of the Poynting flux and soft particle precipitation can cause > 50% neutral density enhancement at 400 km in the cusp region, which is comparable with the CHAMP observations in extreme cases. This study elucidates that both the total geomagnetic energy flux and the altitudinal distribution of this energy, which is influenced strongly by the soft particle precipitation, are of critical significance to increase the neutral density in the cusp.

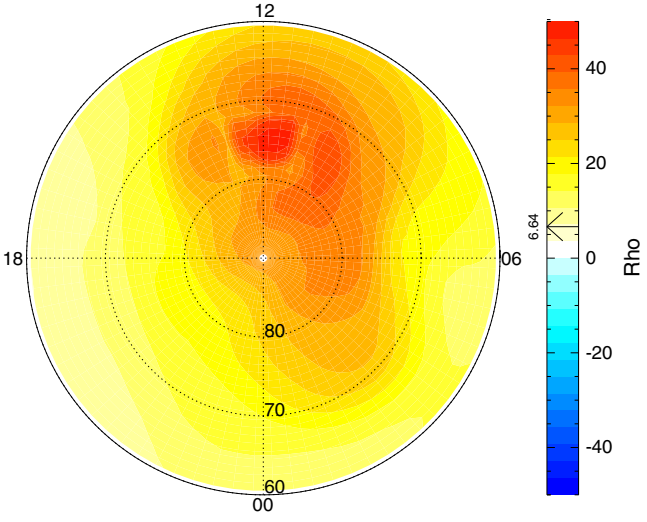

Figure 8. The same as Figure 4 except for the total effect caused by both Poynting flux and soft particle precipitation.

Table 1. Maximum Percentage Change of Neutral Density at 400 km Caused by Different Processes

Energy Source	Input	% Change of ρ_n at 400 km
Poynting flux	75 mW/m^2	34%
Soft electrons (100 eV) heating	2 mW/m^2	5%
Soft electrons (100 eV) ionization	2 mW/m^2	24%
Soft ions (2 keV)	0.3 mW/m^2	–4%
Poynting flux + soft particles	Total	59%

4. Conclusion

[24] We used the Global Ionosphere Thermosphere Model (GITM) to simulate large neutral density enhancement in the cusp for extreme conditions. This study examines the general nature of the thermosphere response to the energy inputs. Several different heating mechanisms including Poynting flux and soft electron and ion particle precipitation have been analyzed to determine their impacts on the neutral density. It is found that a Poynting flux, which is considered to be due to subgrid scale variability not accounted for in statistical models of the ionospheric electric field, of 75 mW/m^2 significantly increases the neutral density at 400 km altitude in the cusp region with the maximum perturbation reaching about 34%. The soft electron precipitation (100 eV and 2 mW/m^2) influences the thermosphere through two processes, direct particle heating and changing the altitudinal distribution of the Joule heating by increasing the ionization and Pedersen conductivity in the F-region. The impact on the neutral density from the second process is dominant, and the total contribution of the soft electron precipitation to the neutral density enhancement at 400 km can be as large as 29%. The effect of soft electrons on the mass density decreases with increasing characteristic energy (with a constant total energy flux) such that 900 eV electrons have negligible influence, while electrons with energy near 100 eV make large contributions to neutral density upheavals. While the soft proton precipitation (2 keV, 0.3 mW/m^2) strongly influences the E-region electron density, the contribution to the neutral density enhancement at 400 km is relatively small (–4%). The comparison reveals that both Poynting flux and soft electron precipitation play significant roles in changing the neutral density in the cusp at 400 km. The combination of these can result in a > 50% neutral density perturbation, which is comparable to the extreme CHAMP satellite measurements. This study concludes that both the total geomagnetic energy flux and the altitudinal distribution of this energy, which is influenced strongly by the soft electron precipitation, are significant in determining the neutral density enhancement in the cusp. It should be noted that dipole tilt angles with respect to the sun were not investigated within this study. The different seasons and UTs that cause varying solar extreme

ultraviolet irradiation of the cusp region may complicate the conclusions made above and will be investigated in further studies.

[25] **Acknowledgments.** This research was supported at the University of Texas by NSF through grant ATM0955629, NASA through grant NNX13AD64G, and AFOSR through Award 1210429, at NCAR by AFOSR MURI award FA9550-07-1-0565, at University of Colorado by grant NNX09AJ88G, at the University of Michigan by NSF grants ANT0838828 and ATM1010812 and through a subcontract from NASA grant NNX09AJ76G to George Mason University. The authors would like to thank Philip Richards for providing revised auroral neutral heating efficiencies, Marina Galand for the use of the empirical model for soft proton precipitation, and Xiaohua Fang for the use of parameterization for the soft electron ionization rate.

References

Aruliah, A. L., et al. (2005), First direct evidence of meso-scale variability on ion-neutral dynamics using co-located tristatic FPIs and EISCAT radar in Northern Scandinavia, *Ann. Geophys.*, *23*, 147–162, doi:10.5194/angeo-23-147-2005.

Bilitza, D. (2001), International reference ionosphere 2000, *Radio Sci.*, *36*, 261.

Burch, J. L. (1968), Low-energy electron fluxes at latitudes above the auroral zone, *J. Geophys. Res.*, *73*, 3585, doi:10.1029/JA073i011p03585.

Carlson, H. C., T. Spain, A. Aruliah, A. Skjaeveland, and J. Moen (2012), First-principles physics of cusp/polar cap thermospheric disturbances, *Geophys. Res. Lett.*, *39*, L19103, doi:10.1029/2012GL053034.

Clemmons, J. H., J. H. Hecht, D. R. Salem, and D. J. Strickland (2008), Thermospheric density in the Earth's magnetic cusp as observed by the Streak mission, *Geophys. Res. Lett.*, *352*, L24,103, doi:10.1029/2008GL035972.

Codrescu, M. V., T. J. Fuller-Rowell, and J. C. Foster (1995), On the importance of E-field variability for Joule heating in the high-latitude thermosphere, *Geophys. Res. Lett.*, *22*, 2393.

Crowley, G., D. J. Knipp, K. A. Drake, J. Lei, E. Sutton, and H. Lühr (2010), Thermospheric density enhancements in the dayside cusp region during strong B_Y conditions, *Geophys. Res. Lett.*, *37*, L07,110, doi:10.1029/2009GL042143.

Demars, H. G., and R. W. Schunk (2007), Thermospheric response to ion heating in the dayside cusp, *J. Atmos. Sol-Terr. Phys.*, *69*, 649–660, doi:10.1016/j.jastp.2006.11.002.

Deng, Y., A. D. Richmond, A. J. Ridley, and H.-L. Liu (2008), Assessment of the non-hydrostatic effect on the upper atmosphere using a general circulation model (GCM), *Geophys. Res. Lett.*, *35*, 1104, doi:10.1029/2007GL032182.

Eather, R. H. (1985), Polar cusp dynamics, *J. Geophys. Res.*, *90*, 1569–1576, doi:10.1029/JA090iA02p01569.

Escoubet, C. P., et al. (2008), Effect of a northward turning of the interplanetary magnetic field on cusp precipitation as observed by Cluster, *J. Geophys. Res. Space Phys.*, *113*, A07S13, doi:10.1029/2007JA012771.

Fang, X., C. E. Randall, D. Lummerzheim, S. C. Solomon, M. J. Mills, D. R. Marsh, C. H. Jackman, W. Wang, and G. Lu (2008), Electron impact ionization: A new parameterization for 100 eV to 1 MeV electrons, *J. Geophys. Res. Space Phys.*, *113*, A09,311, doi:10.1029/2008JA013384.

Fedder, J. A., and J. G. Lyon (1987), The solar wind-magnetosphere-ionosphere current-voltage relationship, *Geophys. Res. Lett.*, *14*, 880.

Fontheim, E. G., L. H. Brace, and J. D. Winningham (1987), Properties of low-energy electron precipitation in the cleft during periods of unusually high ambient electron temperatures, *J. Geophys. Res.*, *92*, 12,267–12,273, doi:10.1029/JA092iA11p12267.

Frey, H. U. (2007), Localized aurora beyond the auroral oval, *Rev. Geophys.*, *45*, RG1003, doi:10.1029/2005RG000174.

Fuller-Rowell, T. J., and D. Evans (1987), Height-integrated Pedersen and Hall conductivity patterns inferred from TIROS-NOAA satellite data, *J. Geophys. Res.*, *92*, 7606.

Fuller-Rowell, T. J., D. Rees, S. Quegan, G. J. Bailey, and R. J. Moffett (1984), The effect of realistic conductivities on the high-latitude neutral thermospheric circulation, *Planet. Space Sci.*, *32*, 469.

Galand, M., and A. D. Richmond (2001), Ionospheric electrical conductances produced by auroral proton precipitation, *J. Geophys. Res.*, *106*, 117–126, doi:10.1029/1999JA002001.

Galand, M., R. G. Roble, and D. Lummerzheim (1999), Ionization by energetic protons in thermosphere-ionosphere electrodynamics general circulation model, *J. Geophys. Res.*, *104*, 27,973–27,990, doi:10.1029/1999JA900374.

Galand, M., T. J. Fuller-Rowell, and M. V. Codrescu (2001), Response of the upper atmosphere to auroral protons, *J. Geophys. Res.*, *106*, 127–140, doi:10.1029/2000JA002009.

Gary, J. B., R. A. Heelis, and J. P. Thayer (1995), Summary of field-aligned poynting flux observations from DE 2, *Geophys. Res. Lett.*, *22*, 1861.

Hardy, D. A., M. S. Gussenhoven, R. Raistrick, and W. J. McNeil (1987), Statistical and functional representation of the pattern of auroral energy flux, number flux, and conductivity, *J. Geophys. Res.*, *92*, 12,275.

Hedin, A. E. (1987), MSIS-86 thermospheric model, *J. Geophys. Res.*, *92*, 4649.

Innis, J. L., and M. Conde (2002), High-latitude thermospheric vertical wind activity from Dynamics Explorer 2 Wind and Temperature Spectrometer observations: Indications of a source region for polar cap gravity waves, *J. Geophys. Res.*, *107*, 1172, doi:10.1029/2001JA009130.

Kelley, M. C., D. J. Knudsen, and J. F. Vickrey (1991), Poynting flux measurements on a satellite–A diagnostic tool for space research, *J. Geophys. Res.*, *96*, 201.

Knipp, D., S. Eriksson, L. Kilcommons, G. Crowley, J. Lei, M. Hairston, and K. Drake (2011), Extreme Poynting flux in the dayside thermosphere: Examples and statistics, *Geophys. Res. Lett.*, *38*, 16102, doi:10.1029/2011GL048302.

Li, W., D. Knipp, J. Lei, and J. Raeder (2011), The relation between dayside local Poynting flux enhancement and cusp reconnection, *J. Geophys. Res. Space Phys.*, *116*, A08,301, doi:10.1029/2011JA016566.

Lühr, H., and S. Marker (2013), High-latitude thermospheric density and wind dependence on solar and magnetic activity, in *Climate and Weather of the Sun-Earth System (CAWSES): Highlights From a Priority Program*, edited by Lübken, F.-J., p. 189, Springer, Dodrecht, The Netherlands.

Lühr, H., M. Rother, W. Köhler, P. Ritter, and L. Grunwaldt (2004), Thermospheric up-welling in the cusp region: Evidence from CHAMP observations, *Geophys. Res. Lett.*, *31*, 6805, doi:10.1029/2003GL019314.

Matsuo, T., and A. D. Richmond (2008), Effects of high-latitude ionospheric electric field variability on global thermospheric Joule heating and mechanical energy transfer rate, *J. Geophys. Res.*, *113*, 7309, doi:10.1029/2007JA012993.

Matsuo, T., A. D. Richmond, and K. Hensel (2003), High-latitude ionospheric electric field variability and electric potential derived from DE-2 plasma drift measurements: Dependence on IMF and dipole tilt, *J. Geophys. Res.*, *108*, 1005, doi:10.1029/2002JA009429.

Millward, G. H., R. J. Moffett, H. F. Balmforth, and A. S. Rodger (1999), Modeling the ionospheric effects of ion and electron precipitation in the cusp, *J. Geophys. Res.*, *104*, 24,603–24,612, doi:10.1029/1999JA900249.

Newell, P. T., and C.-I. Meng (1987), Cusp width and B(z)–Observations and a conceptual model, *J. Geophys. Res.*, *92*, 13,673–13,678, doi:10.1029/JA092iA12p13673.

Newell, P. T., and C. I. Meng (1992), Mapping the dayside ionosphere to the magnetosphere according to particle precipitation characteristics, *Geophys. Res. Lett.*, *19*, 609.

Newell, P. T., C.-I. Meng, D. G. Sibeck, and R. Lepping (1989), Some low-altitude cusp dependencies on the interplanetary magnetic field, *J. Geophys. Res.*, *94*, 8921–8927, doi:10.1029/JA094iA07p08921.

Newell, P. T., K. Liou, and G. R. Wilson (2009), Polar cap particle precipitation and aurora: Review and commentary, *J. Atmos. Sol-Terr. Phys.*, *71*, 199–215, doi:10.1016/j.jastp.2008.11.004.

Potemra, T. A., C. O. Bostrom, R. W. McEntire, W. K. Peterson, J. P. Doering, and R. A. Hoffman (1977), Low-energy particle observations in the quiet dayside cusp from AE-C and AE-D, *J. Geophys. Res.*, *82*, 4765–4776, doi:10.1029/JA082i029p04765.

Prölss, G. W. (2006), Electron temperature enhancement beneath the magnetospheric cusp, *J. Geophys. Res. Space Phys.*, *111*, A07,304, doi:10.1029/2006JA011618.

Rees, M. H., B. A. Emery, R. G. Roble, and K. Stamnes (1983), Neutral and ion gas heating by auroral electron precipitation, *J. Geophys. Res.*, *88*, 6289–6300.

Reigber, C., H. Lühr, and P. Schwintzer (2002), CHAMP mission status, *Adv. Space Res.*, *30*, 129.

Rentz, S. (2009), The upper atmospheric fountain effect in the polar cusp region, Ph.D. Thesis.

Rentz, S., and H. Lühr (2008), Climatology of the cusp-related thermospheric mass density anomaly, as derived from CHAMP observations, *Ann. Geophys.*, *26*, 2807–2823, doi:10.5194/angeo-26-2807-2008.

Richards, P. J. (2013), Reevaluation of thermosphere heating by auroral electrons, *Adv. Space Res.*, *51*, 610, doi:10.1016/j.asr.2011.09.004.

Richmond, A. D. (1992), Assimilative mapping of ionospheric electrodynamics, *Adv. Space Res.*, *12*, 59.

Richmond, A. D. (2010), On the ionospheric application of Poynting's theorem, *J. Geophys. Res. Space Phys.*, *115*, 10,311, doi:10.1029/2010JA015768.

Ridley, A. J., T. I. Gombosi, and D. L. D. Zeeuw (2004), Ionospheric control of the magnetospheric configuration: Conductance, *Ann. Geophys.*, *22*, 567, doi:10.5194/angeo-22-567-2004.

Ridley, A. J., Y. Deng, and G. Toth (2006), The global ionosphere-thermosphere model, *J. Atmos. Sol-Terr. Phys.*, *68*, 839, doi:10.1016/j.jastp.2006.01.008.

Roble, R. G., and E. C. Ridley (1987), An auroral model for the NCAR thermospheric general circulation model (TGCM), *Ann. Geophys.*, *5A*, 369.

Roble, R. G., E. C. Ridley, and R. E. Dickinson (1987), On the global mean structure of the thermosphere, *J. Geophys. Res.*, *92*, 8745.

Schlegel, K., H. Lühr, J.-P. S. -Maurice, G. Crowley, and C. Hackert (2005), Thermospheric density structures over the polar regions observed with CHAMP, *Ann. Geophys.*, *23*, 1659–1672, doi:10.5194/angeo-23-1659-2005.

Schunk, R. W., and A. F. Nagy (2000), *Ionospheres*, Cambridge University Press, Cambridge, U. K.

Schunk, R. W., and A. F. Nagy (2009), *Ionospheres*, 2nd ed., Cambridge University Press, Cambridge, U. K.

Smith, M. F., and M. Lockwood (1996), Earth's magnetospheric cusps, *Rev. Geophys.*, *34*, 233–260, doi:10.1029/96RG00893.

Smith, R. W., and G. Hernandez (1995), Vertical winds in the thermosphere within the polar cap, *J. Atmos. Terr. Phys.*, *57*, 611–620.

Thayer, J. P., J. F. Vickrey, R. A. Heelis, and J. B. Gary (1995), Interpretation and modeling of the high-latitude electromagnetic energy flux, *J. Geophys. Res.*, *100*, 19,715.

Vickrey, J. F., R. R. Vondrak, and S. J. Matthews (1982), Energy deposition by precipitating particles and Joule dissipation in the auroral ionosphere, *J. Geophys. Res.*, *87*, 5184.

Vontrat-Reberac, A., D. Fontaine, P.-L. Blelly, and M. Galand (2001), Theoretical predictions of the effect of cusp and dayside precipitation on the polar ionosphere, *J. Geophys. Res.*, *106*, 28,857–28,866, doi:10.1029/2001JA900131.

Weimer, D. R. (1996), A flexible, IMF dependent model of high-latitude electric potential having "space weather" applications, *Geophys. Res. Lett.*, *23*, 2549.

Weimer, D. R. (2005), Improved ionospheric electrodynamic models and application to calculating Joule heating rates, *J. Geophys. Res.*, *110*, 5306, doi:10.1029/2004JA010884.

Wu, Q., W. Wang, R. G. Roble, I. Häggström, and A. Strømme (2012), First daytime thermospheric wind observation from a balloon-borne Fabry-Perot interferometer over Kiruna (68N), *Geophys. Res. Lett.*, *39*, L14104, doi:10.1029/2012GL052533.

Yiğit, E., and A. J. Ridley (2011), Effects of high-latitude thermosphere heating at various scale sizes simulated by a nonhydrostatic global thermosphere-ionosphere model, *J. Atmos. Sol-Terr. Phys.*, *73*, 592–600, doi:10.1016/j.jastp.2010.12.003.

Yordanova, E., et al. (2007), Energy input from the exterior cusp into the ionosphere: Correlated ground-based and satellite observations, *Geophys. Res. Lett.*, *340*, L04,102, doi:10.1029/2006GL028617.

Zhang, B., W. Lotko, O. Brambles, M. Wiltberger, W. Wang, P. Schmitt, and J. Lyon (2012), Enhancement of thermospheric mass density by soft electron precipitation, *Geophys. Res. Lett.*, *39*, L20102, doi:10.1029/2012GL053519.

Zhou, X. W., C. T. Russell, G. Le, S. A. Fuselier, and J. D. Scudder (2000), Solar wind control of the polar cusp at high altitude, *J. Geophys. Res.*, *105*, 245–252, doi:10.1029/1999JA900412.